The impact of observation nudging on simulated meteorology and ozone concentrations during DISCOVER-AQ 2013 Texas campaign

Xiangshang Li [1], Yunsoo Choi [1], Beata Czader [1], Anirban Roy [1], Hyuncheol Kim [2,3], Barry Lefer [1], Shuai Pan [1]

[1]Department of Earth and Atmospheric Sciences, University of Houston, Houston, TX, 77204, USA

[2]NOAA Air Resources Laboratory, College Park, MD 20740, USA

[3]University of Maryland, Cooperative Institute for Climate and Satellite, College Park, MD, USA

Corresponding author: Xiangshang Li: xli@central.uh.edu

Abstract

Accurate meteorological fields are imperative for correct chemical transport modeling. Observation nudging, along with objective analysis, is generally considered as a low-cost and effective technique to improve meteorological simulations. However, the meteorological impact of observation nudging on chemistry has not been well characterized. This study involved two simulations to analyze the impact of observation nudging on the simulated meteorology and ozone concentrations during the 2013 Deriving Information on Surface conditions from Column and Vertically Resolved Observations Relevant to Air Quality (DISCOVER-AQ) Texas campaign period, using Weather Research and Forecasting (WRF) and Community Multiscale Air Quality (CMAQ) models. The results showed improved correlations between observed and simulated parameters from the sensitivity case. The index of agreement (IOA) improved by about 9% for surface temperature and 6-11% for surface zonal (U-WIND) and meridional (V-WIND) winds when observation nudging was employed. Analysis of a cold front event indicated that it improved the timing of wind transition during the front passage. Employing observation

nudging also reduced the model biases for the planetary boundary height predictions. For CMAQ simulations, the IOA improved by 6% in the sensitivity case for surface ozone during the entire simulation period. The high ozone episode on September 25th was a post-front ozone event in Houston. The small-scale morning wind shifts near the Houston Ship Channel combined with higher aloft ozone early morning likely caused the day's ozone exceedance. While observation nudging did not recreate the wind shifts on that day and failed to reproduce the observed high ozone, analyses of surface and aircraft data found that observation nudging helped model to yield improved ozone predictions. In a two-hour period during the event, substantially better winds in the sensitivity case noticeably improved the ozone. Further work on improving the capability of nudging to reproduce local meteorological events could enhance a chemical transport model's capability to predict high ozone events.

Keywords: WRF, CMAQ, air quality model, DISCOVER-AQ, observation nudging

1. Introduction

Meteorological variables such as cloud fraction, winds, planetary boundary layer (PBL) heights and precipitation significantly impact air quality. They influence the production, transport, and deposition of various chemical species (e.g., Pour-Biazar et al. 2007; Banta et al. 2005; Cuchiara et al. 2014). Hence accurate meteorological inputs are imperative for air quality modeling. Common approaches of improving meteorological simulations include the selection of updated and high resolution terrain data (e.g., Cheng and Byun 2008), optimization of physics and dynamics options (e.g., Zhong et al. 2007) and the implementation of four dimensional data assimilation (FDDA).

FDDA continuously merges new observational data into model simulation such that the model's predictions do not drift away from observations. There are several FDDA methods including nudging (e.g., Stauffer and Seaman 2004) and Variational Methods (3D-VAR or 4D-VAR; e.g., Le Dimet and Talagrand 1986; Huang et al. 2009). 4D-VAR obtains optimal states of the atmosphere using multi-time-level observations by globally adjusting a model solution to all available observations over an interval of time. Nudging is a simple yet flexible FDDA method originally developed by Stauffer and Seaman (1990, 1994), and implemented in the Fifth-

Generation PSU/NCAR Mesoscale Model (MM5). Not intended for optimal adjustment, nudging is less computationally intensive but needs special care for the nudging coefficients. Nudging involves adding an artificial tendency term to one or more model prognostic equations that reflect the difference between the best estimate of the observed state and the model state at a given location and time. In short, the goal is to "nudge" model state towards observed state. There are several types of nudging such as 3D analysis nudging, surface analysis nudging, and observation nudging (obs-nudging). In the case of analysis nudging, the model state is nudged toward gridded analysis. The difference between 3D and surface analysis nudging is that 3D analysis (at all model levels except for surface) data are used to improve 3D fields while surface analysis data are used to improve surface fields. In observation nudging, the model predictions are nudged to match better with observations at individual locations both surface and aloft. The MM5 nudging codes were later improved and incorporated into the Weather Research and Forecasting (WRF) model by Liu et al. (2005, 2006). The enhancements enable obs-nudging to assimilate a large variety of direct or derived observations. In WRF, the inputs for obs-nudging are generated by WRF OBSGRID program. This program also performs Objective Analysis (OA) to improve the quality of analysis nudging files. Objective Analysis updates first guess meteorology analysis by incorporating observational data. Since obs-nudging is usually performed along with OA (as in this study) to maximize the benefits of assimilating observations, we also use OA to denote the combined Objective Analysis and obs-nudging processes in case names.

The benefit of applying nudging to improve meteorological simulations has been demonstrated in many studies (e.g., Deng 2009; Gilliam and Pleim 2010). However, the impact of the improved fields on air quality simulations has been investigated by relatively fewer studies. Otte (2008) showed that the Community Multiscale Air Quality (CMAQ) model with improved MM5 meteorology using analysis nudging was able to better simulate ozone chemistry as reflected in model-measurement statistics. Their results indicated that better "model skill" scores were achieved for daily maximum 1-hr ozone mixing ratios after analysis nudging over a 35-day simulation episode. Byun et al. (2008) performed over a dozen tests on obs-nudging (with analysis nudging turned on) and showed obs-nudging improved both winds and temperature in MM5 simulations. The study also gave an example in which improved wind fields on a given day helped the CMAQ model better capture the ozone hotspot southwest of Houston. Ngan et al.

(2012) compared results from several CMAQ simulations coupled to the MM5 model which included nudging. Their results indicated that fully nudged (with both analysis nudging and obs-nudging implemented) simulations performed better with respect to both meteorology and ozone chemistry. However, the statistics from their study cannot be used for interpreting the sensitivity of obs-nudging since its base WRF case is a forecast run which used a different analysis input. Previous studies by the current authors (e.g., Rappenglueck et al. 2011; Czader et al. 2013) showed that obs-nudging helped correct errors in model wind fields, critical to the transport of pollutants and production of secondary pollutants. To the best of the authors' knowledge, there is no comprehensive study on the impact of obs-nudging on air quality simulation using the WRF model.

This study intends to fill up the gap in the studies mentioned above by investigating the sensitivity of WRF and subsequently, CMAQ simulations to observation nudging. In theory, higher frequency of obs-nudging input should have a higher probability to capture small scale events, such as local wind shifts. These events may only slightly impact local weather, yet have a marked effect on chemistry. This is because local stagnation and wind convergence/reversals can contribute to the pollutant build-up, as indicated by Banta et al. (1998), Cheung and Wang (2001) and Tucker et al. (2010).

There is a significant presence of petrochemical facilities, power plants and motor vehicles in the Houston-Galveston-Brazoria (HGB) region located in southeastern Texas (SETX). The major pollutant in the region is ozone due to the abundant emissions of precursors like nitrogen oxide (NO_x) and Volatile Organic Compounds (VOCs). During the long and hot summer, ozone concentrations often rise above the National Ambient Air Quality Standard (NAAQS). Consequently, HGB has been designated as an ozone nonattainment region by the US Environmental Protection Agency (USEPA) (http://www3.epa.gov/airquality/greenbook/hncs.html#TEXAS). The petrochemical plants are largely concentrated in the Houston Ship Channel (HSC) area - just north of the Galveston Bay. The VOCs emitted from the HSC area are highly reactive and have been shown to contribute greatly to the high regional ozone episodes (e.g. Kleinman et al. 2002; Daum et al. 2003). Depending on the local meteorology, the plumes from HSC may be carried to different locations in HGB and trigger high ozone events on its path. Metropolitan Houston has a high level of NO_x

emissions partly due to heavy vehicular traffic in the city. As a result of the large amount of precursor emissions and favorable weather, relatively frequent high ozone events occur in the area.

Due to the reasons listed above, the Houston-Galveston-Brazoria region has been the focus of several air quality studies in the recent past (e.g., Banta et al. 2005; Parrish et al. 2009; Lefer and Rappengluck 2010; Olaguer et al. 2013; Czader et al. 2013, Choi et al. 2012; Choi 2014; Choi and Souri, 2015; Pan et al. 2015). It is a good place for studying ozone production and transport due to the existence of a dense surface monitoring network, as well as several intensive measurement field campaigns which provide ample observational data. For example in September 2013, the National Aeronautics and Space Administration (NASA), joined by a number of agencies and universities, conducted a field measurement campaign in SETX as part of its the Deriving Information on Surface conditions from Column and Vertically Resolved Observations Relevant to Air Quality (DISCOVER-AQ) program (http://www-air.larc.nasa.gov/missions/discover-aq/discover-aq.html). This program has conducted several air quality and meteorology measurements at different locations in the U.S. The availability of dense surface observations is important for obs-nudging to correct erroneous local winds in the model. The performance of obs-nudging will be handicapped without a rich set of observations.

This study involved performing two sets of WRF and CMAQ model simulations for the 2013 DISCOVER-AQ Texas time period in order to understand the impact of obs-nudging. The data for nudging included multiple sets of observation data from both surface and aloft measurements. We evaluated model-measurement performance statistics for both WRF and CMAQ output.

2. Observational Data and Model Configurations

2.1 Observational Data

This study used regular measurements from the Continuous Ambient Monitoring Stations (CAMS) operated by the Texas Commission on Environmental Quality (TCEQ). Additionally, PBL and aloft ozone measurement data were obtained from the DISCOVER-AQ campaign. For observation nudging, CAMS data and several data streams from the Meteorological Assimilation Data Ingest System (MADIS) were used. The CAMS measurement network collected real-time meteorology and pollutant data. The measured parameters differ from station to station. The

station density at South East Texas (SETX) is relatively high. There were 63 sites with meteorological and 52 sites with ozone measurements in the 4-km domain. The network is represented in Figure 1. The sites are represented by dots, with the La Porte (C556) site labeled. All CAMS observations are accessible at TCEQ website: http://www.tceq.state.tx.us/cgi-bin/compliance/monops/daily_summary.pl.

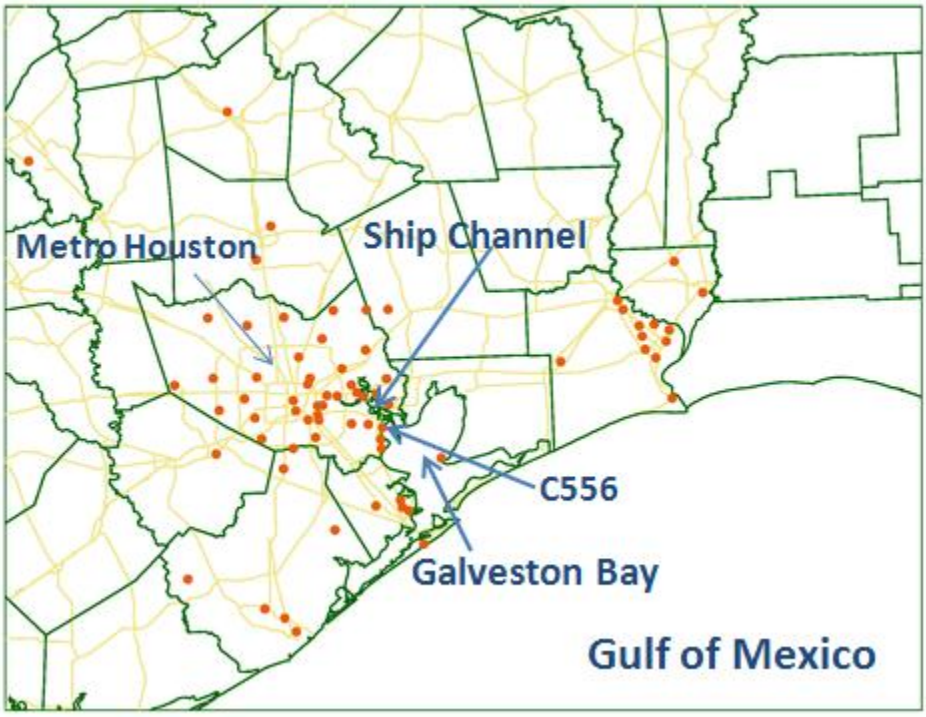

Figure 1. Locations of CAMS sites (dots) in CMAQ 4-km modeling domain during September 2013. Metro Houston, Houston Ship Channel, Galveston Bay and Gulf of Mexico are labeled.

Additionally, PBL height measurements for September were recorded at a site at the University of Houston. The PBL height was measured using the Light Detection and Ranging (LIDAR) system. The PBL data is currently available only at this site. For analysis of aloft ozone, we also used measurements from aircraft P-3B, part of the rich datasets collected during DISCOVER-AQ campaign. The P-3B data had over 100 parameters which are accessible online.

2.2 Model Configurations

The modeling system consists of the WRF meteorological model (Skamarock et al., 2008), the Sparse Matrix Operator Kernel Emissions (SMOKE) model for emissions modeling (Houyoux et

al., 2000) and the CMAQ model (Byun and Schere, 2006) for chemical transport modeling. The details about model configurations are presented in the following sections. Two sets of simulations were conducted, one set with obs-nudging and OA and the other without. The base case, referred as "No-OA", did not employ obs-nudging or OA. The second case, "1Hr-OA", performed obs-nudging and OA using hourly nudging input.

2.2.1. WRF Setup

Both WRF simulations used the same nested domain and NARR (North American Regional Reanalysis) as input, with grid nudging turned on. Figure 2 depicts the horizontal domain setup. Two nested domains were used, with 12-km and 4-km resolution respectively. The 4-km domain covered SETX and a small portion of Louisiana. The 12-km domain (red box) encompassed Texas and parts of a few neighboring states. The number of grid cells for the 12-km and 4-km domains were 161×145 (E-W by N-S), and 95×77 respectively. The projection type was Lambert conic conformal (LCC). Three projection parameters were considered: namely first latitude (33 °N), second latitude (45 °N) and standard longitude (97 °W). The USEPA used the same projection parameters to develop emission inventories for air quality modeling (Mason et al. 2010). Both domains had a vertical resolution of 27 eta layers based on dry hydrostatic pressures. The model top is 100 hPa, corresponding to top layer pressure of the input NARR data.

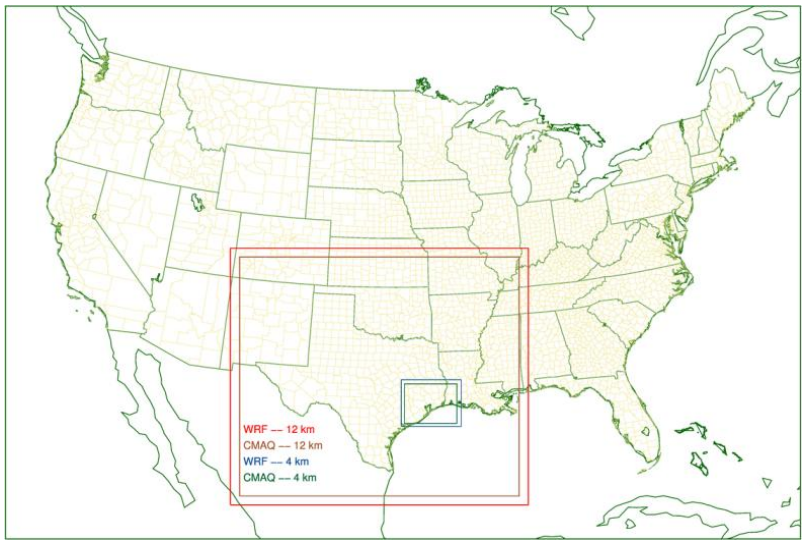

Figure 2. Horizontal domains of WRF and CMAQ simulation at 4 km and 12 km grid resolution (the bigger domains are for 12 km WRF and CMAQ and the smaller domains for 4 km WRF and CMAQ).

2.2.1.1. Input Data

The NARR data used for WRF simulations is downloadable from http://rda.ucar.edu/datasets/ds608.0/. The data were based on an Eta 221 grid at 29 pressure levels. Its horizontal resolution was 32-km and the frequency was 3 hourly. The initial and boundary conditions were generated from the NARR analysis by WRF. An alternative to NARR was the Eta-NAM analysis data. However, the data temporal frequency was lowered from 3-hourly to 6-hourly starting 2013. Our tests showed that it was not as good as NARR dataset - likely because of lower temporal resolution.

2.2.1.2. Physics and FDDA Options

Major physics options used in the model are listed in Table 1. Our past modeling experiences indicated that employing the Yonsei University (YSU) for PBL scheme and the Kain-Fritsch (K-F) for cumulous scheme gave the best results for the Houston area. YSU scheme was also one of the two PBL schemes recommended by Cuchiara et al. (2014). The K-F scheme is "drier" than others and produces less number of "false" convectional thunderstorms. For grid nudging options, we generally followed the recommendations in the WRF's User Guide. For example, the mass fields (temperature and moisture) were nudged only at layers above the PBL while wind fields were adjusted at all layers including the surface layer.

2.2.1.3. Observation Nudging with MADIS and CAMS data in WRF

Additional observational data are required to implement obs-nudging and OA. To generate the input files for the OBSGRID program, we processed the observation data using the approach of Ngan et al. (2012) and Czader et al. (2013). Observational data came from the MADIS and TCEQ CAMS. MADIS is a National Oceanic and Atmospheric Administration (NOAA) program which collects, integrates, quality-controls and distributes observations from NOAA and other organizations. Additional information is available online, https://madis.ncep.noaa.gov/. The four MADIS datasets used for obs-nudging were NOAA Profiler Network (NPN),

Cooperative Agency Profilers (CAP), Meteorological Terminal Aviation Routine (METAR) weather report and NOAA Radiosonde (RAOB). The METAR dataset was collected by mostly first-order, METAR reporting, surface monitoring stations. NPN, RAOB and CAP were the most commonly used upper air datasets.

The processed input observation data were fed into OBSGRID to update the domain analyses and generate additional surface analyses and text nudging files. Actual obs-nudging was performed by the main WRF program after obs-nudging namelist variables are properly set. The namelist for OBSGRID and relevant WRF section settings came largely from recommended values of WRF User's Guide and a previous study by Ngan et al. (2012).

Theoretically, obs-nudging updating at a higher frequency should enhance the model's performance. A typical frequency of input analysis data is 3-hourly while the frequency for observational data is hourly. The 3-hourly frequency of input analyses may be the reason for the default 3-hour time interval in WRF's OBSGRID settings for generating the obs-nudging files. Since there were few existing obs-nudging studies related to air quality and we are not aware of any reference to the adoption of 1-hour input frequency, we assume that all the existing studies used the default 3-hour interval. As the WRF model allows the interval to be set to 1-hour or smaller when corresponding observational data were available, we tested both 1-hour and 3-hour scenarios. The results indicated that 1-hour obs-nudging had slightly better performance than the 3-hour one. As a result, this study adopted 1-hour temporal frequency for observation nudging. The quantities that were nudged were temperature, moisture, and the two wind components (U-WIND and V-WIND). Obs-nudging for moisture was not performed in this study. This was based on our past experiences since performing moisture nudging sometimes trigger excessive artificial thunderstorms which disrupted model flow fields.

2.2.2. Emissions Processing

For anthropogenic sources we utilized the National Emissions Inventory of 2008 (NEI2008) generated by the USEPA (USEPA, 2011). Motor vehicle emissions for this inventory were processed using the EPA's Motor Vehicle Emissions Simulator (MOVES) (USEPA, 2015). The inventory was processed using the Sparse Matrix Operator Kernel Emissions (SMOKE) model v3.1 to obtain gridded emission rates and speciated for the Carbon Bond 05 (CB05) chemical

mechanism for use in the CMAQ model. The biogenic emissions were modeled using the Biogenic Emissions Inventory System (BEIS) v3.14. Although NEI2008 might have overestimated NO_x emissions in Houston (e.g., Choi 2012; Czader et al. 2015), we used base NEI2008 without adjustment because the adjustment of the NO_x emission also has large uncertainty. Pan et al. (2015) showed that the CMAQ ozone performance using NEI2008 appears reasonable.

2.2.3. CMAQ Configurations

The USEPA's CMAQ (Byun and Schere 2006) version 5.0.1 was adopted for this study. Several air quality studies focusing on the Houston area have used this model (e.g., Foley et al. 2010; Czader et al. 2013, 2015; Choi 2014; Pan et al. 2015). CMAQ horizontal domains were slightly smaller than the WRF counterpart in order to avoid the discontinuity near the domain boundary. The domains were shown in Figure 2 as green and brown boxes. The chemical boundary conditions for all the species in the 4-km domain were derived from 12-km domain air quality forecasting results (http://spock.geosc.uh.edu). The model used the same vertical structure as WRF. Major CMAQ configurations are listed in Table 2. Chemical processes were simulated with the available in CMAQ CB05 chemical mechanism with cloud/aqueous chemistry, active chlorine chemistry and updated toluene mechanism. For aerosol modeling, the fifth-generation CMAQ aerosol mechanism (AE5) which includes sea salt modeling was selected. The total number of included species is 132, with 70 reactive gas-phase, 49 aerosol and 13 non-reactive species.

3. Evaluation Metrics

To assess model performance against observations, we computed a set of five statistics including Pearson correlation, index of agreement (IOA, Willmott 1981), mean bias (MB), root mean square error (RMSE), and Mean Absolute Error (MAE). This list is similar to one used by Li et al (2008) for model performance evaluation. The goal is to have a comprehensive comparison between model and observation time series. The set of five statistics was divided into three groups:

1) Evaluation of the magnitude of model results vis-a-vis in-situ data

- Mean Bias (MB)
- Mean Absolute Error (MAE)
- Root Mean Square Error (RMSE)

2) Measuring how close the model values follow changes in the observations, unitless

- Correlation

3) A composite performance index, index of agreement (IOA or d), unitless

IOA is considered a better performance index than correlation as it takes into account the difference in the means and standard deviation. For example, when correlations are similar, lower model biases would yield higher IOA values. Additionally, the mean and the standard deviation of model values and observations were included as a reference.

4. General Meteorological and Ozone Conditions in September 2013

The weather during September 2013 was relatively dry with mostly southerly, easterly or southeasterly winds. From 5 to 19 September, there was a lack of influence of strong synoptic weather systems. Shifting wind patterns were observed during the period: light northeasterly in the early morning gradually turned clockwise to southeasterly in the afternoon and evening hours. In this period, winds shifted from southeast to near east and there were more clouds after 10 September. The only cold front arrived on the early morning of 21 September. Figure 3 shows the regional average temperatures for the period and it can be seen that 21 September has the lowest daily high temperature. The influences of the cold air intrusion lasted till early 25 September. Winds turned into southerly in the afternoon of the 25th and warming continued in the next few days until the 28th.

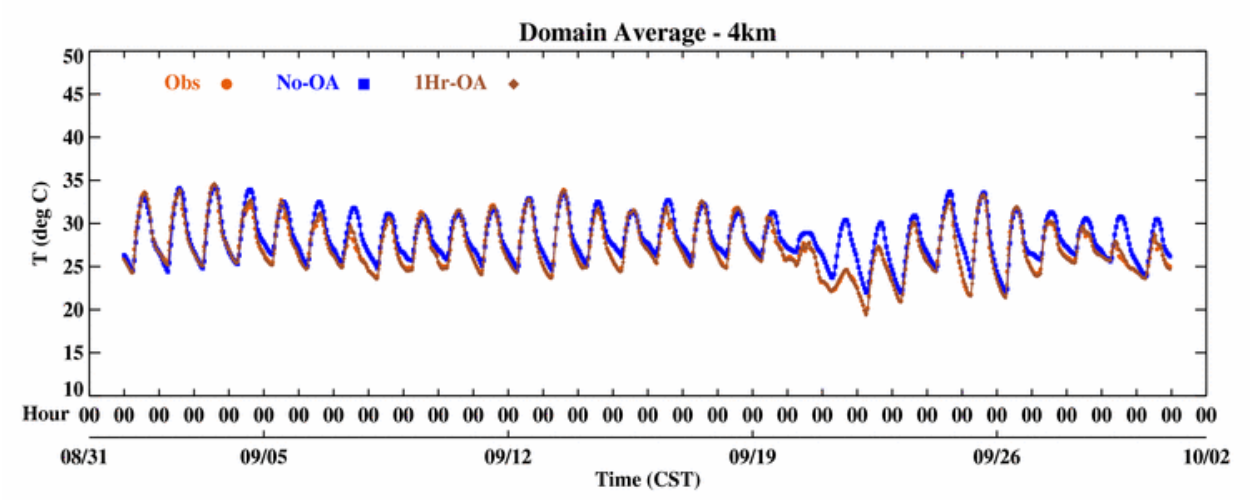

Figure 3. Regional hourly temperature averaged over all available hourly CAMS observations, two model cases also included for September of 2013.

Light rain events occurred on 09/02, 09/10, 09/16, 09/19 to 09/21 and 09/28 to 09/30. The 09/20 and 09/21 events consisted of widespread light to medium showers. Besides the above-mentioned dates, there were a few other days with sporadic drizzles. A majority of the days between 09/01 and 09/20 were either sunny or cloudy. The periods from 09/08 to 09/10 and 09/18 to 09/20 had more clouds than other days. The period from 09/21 to 09/30 was influenced by a cold front passage. The days between 09/22 and 09/24 were sunny and cold. The surface wind reversed direction during midday of 09/25 and brought clouds back from 09/26 to 09/30. High ozone events in SETX during fall are typically associated with a passage of cold front (e.g., Rappenglueck et al. 2008). The only ozone event with hourly surface ozone exceeding 120 ppb (parts per billion) in September which occurred on the 25th fell in this category.

Figure 4 plots the hourly regional averaged ozone. On most days, the in-situ averaged ozone concentrations were below 70 ppb. Since the winds after dawn consistently pushed the precursors from the industrial area to the southwest of the city, the wind pattern did not favor the local ozone production. The daytime winds also contained a persistent easterly component which moved the pollutants away from the Houston metropolitan area. In the first 10-day period, low background ozone originating from the Gulf of Mexico contributed to the low-ozone days. With overcast skies on the 19th and the 20th, hourly high ozone values dipped below 30 ppb. The two highest ozone days characterized by post-frontal ozone events were the 25th and the 26th.

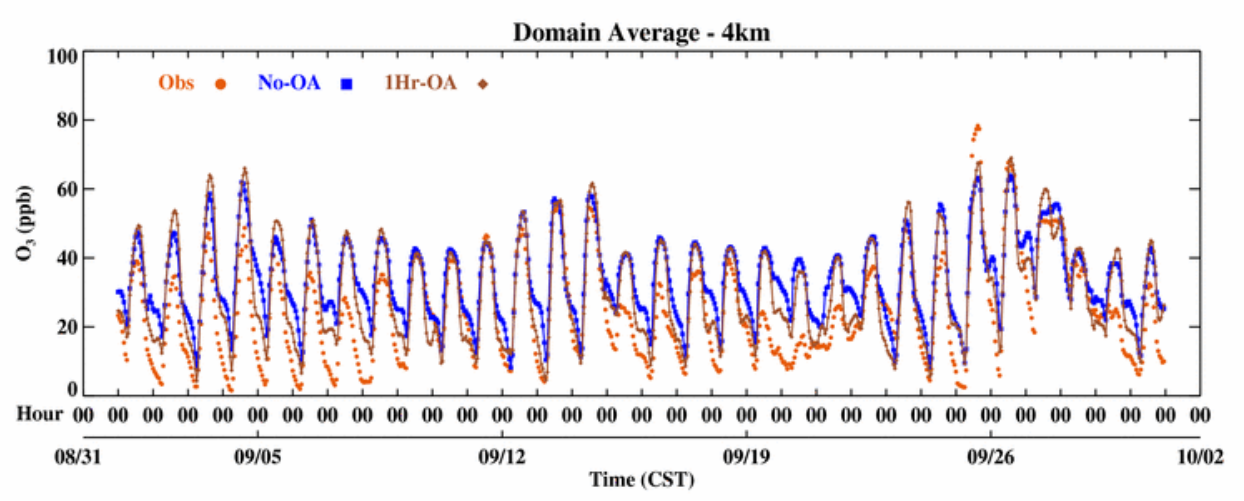

Figure 4. The hourly regional averaged ozone for the two cases (No-OA and 1hr-OA) at the stations which include observation surface O_3 over the 4km domain for September of 2013.

5. Results

To evaluate the WRF simulation, we calculated statistics for surface temperature and winds in the 4-km domain. For PBL heights, we chose to plot out the time-series for the one site we had observations due to significant amount of missing data (data coverage is about 50%). For CMAQ evaluation, we calculated the surface ozone statistics for the whole month. Also, we plotted vertical ozone profile and calculated biases for aloft ozone on the 25th.

5.1. Meteorology

5.1.1. Temperature

The comparison of regional average hourly temperature for the simulation period is shown in Figure 3. The regional observed averaged surface temperature was calculated by averaging the hourly temperature from ~60 CAMS sites in the 4-km model domain. The base case temperature was too high compared to the in-situ measurements. For example, the No-OA maximum temperature for the 21st was 30^{o}C compared to 25^{o}C for the in-situ data. The high biases in the base case are sharply reduced in the "1Hr-OA" case and temperature matched better with the observations for several time periods, especially for September 20-23. The statistics of hourly surface temperature are listed in Table 3. With higher IOA and lower mean biases (MB), the

"1Hr-OA" case was clearly better than the base case "No-OA". The IOA of "1Hr-OA" was about 9% higher than the base case.

5.1.2. Winds

In ozone chemistry, winds affect the accumulation of precursors and hence the resulting ozone production (e.g., Banta et al. 2005, 2011; Darby 2005). They are also responsible for dispersing high ozone and bringing in background ozone. Prevailing summer time southerly to southeasterly winds in the HGB region significantly lower the ozone concentrations in the metropolitan area. Therefore, high ozone events usually occur when such wind patterns change. Cold front intrusions coming as early as late August blow pollutants to the south. As a result, an area of high ozone develops in the Gulf. Following cold fronts weakening and the weather warming up, reversing winds can bring high ozone back to land. High ozone may also occur during intra-day recirculation events when pollutants previously blown away from industrial zone are brought back by reversing winds. Correctly simulating these recirculation events is particularly important in predicting the high ozone event caused by post-front conditions. The ozone event in the HSC area on 09/25 was likely due to a combination of local recirculation caused by onset of the bay breeze and increased background ozone brought in by transport.

Due to the land-water thermal contrast and the different size of the Galveston Bay and the Gulf of Mexico, the western shore of the Galveston Bay often experiences a successive onset of bay breeze and sea breeze in the summer. The bay breeze is typically a weaker easterly while sea breeze is a stronger southeasterly. Sea breeze usually comes one to a few hours later after the bay breeze. The bay breeze and the subsequent sea breeze phenomena in Houston were described by Banta et al. (2005).

The statistics of zonal (U-WIND) and meridional (V-WIND) wind components are listed in Table 3. The purpose of choosing U and V over wind speed and direction is to avoid the anomalies in the wind direction statistics. For example, although wind direction of 5 and 355 degrees are close, the statistics suggest that they are distinctively different.

For both U and V components of wind, "1Hr-OA" had higher correlation and IOA than "No-OA". The model performance on U and V are similar, with the correlation in a range of 0.76 to 0.81 for all the cases. For comparison, the performance of the OA case ("M1") in Ngan et al.

(2012) is very close to that in this study, with a correlation of 0.75 for U and 0.82 for V. In terms of IOA, the OA case had a larger lead over the base case, ahead by 5-6% in U and 10-11% in V over the base case. This can be explained by the much reduced wind biases in the OA case.

The base case had consistently stronger winds, especially the southerly component, than the observation. This was reflected in the mean bias "MB", as well as the model mean "M_M". Winds were reduced significantly after OA was performed. Interestingly, the high southerly bias in "No-OA" turned slightly negative after OA. Winds originating from the Gulf were also stronger in base case, which played a role in raising the ozone level comparing to the sensitivity case. Figure 5 illustrated the slowing down of southerly winds after observation nudging. As a result of nudging, the wind vectors matched better to the observations.

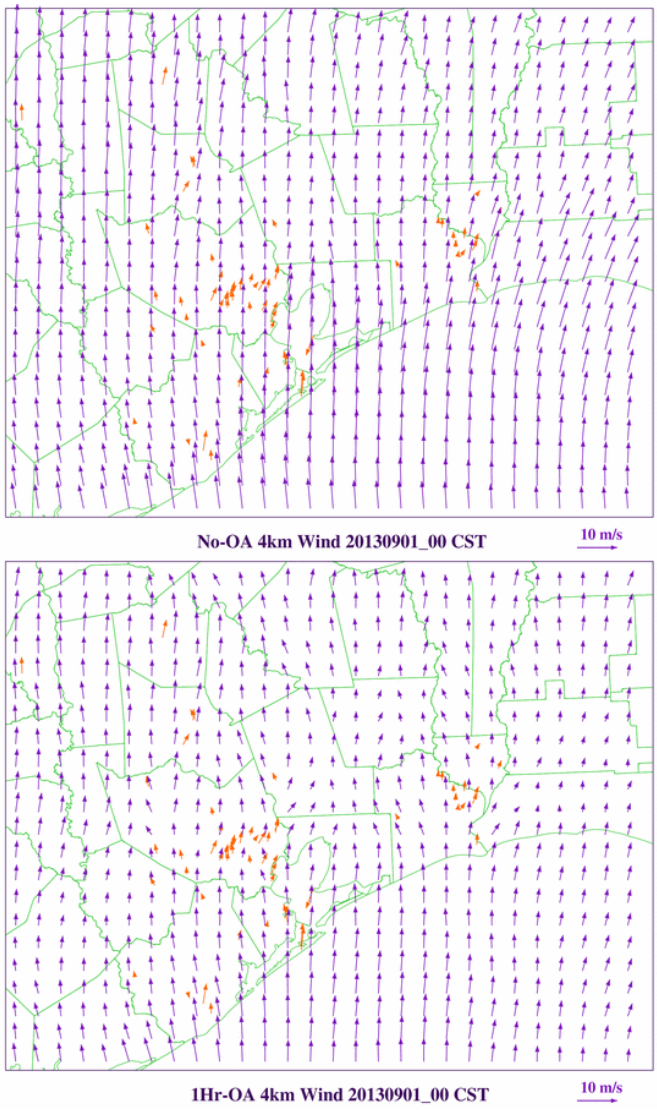

Figure 5. Model and observed winds at 09/01_00 CST: No-OA (top) and 1Hr-OA (bottom). Model winds are blue arrows and the observations are orange arrows. Stronger southerly winds, especially along coastal region, were reduced in the OA case.

5.1.3. PBL height

Atmospheric pollutants are largely confined in the PBL as most of the emissions sources are close to the ground level. Hence the PBL height plays a critical role in mixing and spreading the pollutants. Haman et al. (2014) studied the relationship between ozone level and PBL height at a Houston CAMS site and found that nighttime and early morning PBL heights were consistently lower on high ozone days than on low ozone days. Czader et al. (2013) pointed out that the model underprediction of PBL during nighttime may have caused the CO overprediction at the same site. CO is a good proxy for understanding model's transport since it has low reactivity and a relatively long life time in the troposphere. Cuchiara el al. (2014) conducted four WRF/Chem sensitivity tests using different PBL schemes over southeast Texas. While no preferred PBL scheme was identified for WRF simulations, the YSU scheme performed better than others in terms of ozone prediction.

Haman et al. (2012) showed that the daily maximum PBL height at the University of Houston site indicated previously reached its highest values of slightly over 2000 m in August. In September, typical daily maximum PBL height was 1500 m at 15 CST while daily minimum was just below 200 m between 00 CST and 06 CST. The comparison of observed and model PBL height is shown at Figure 6. Our results indicated that the model tended to overpredict the daily maximum PBL height; obs-nudging helped to reduce the overprediction. For the daily minimum PBL height, "No-OA" case had slightly high biases while the OA case matched quite well with in-situ height data. The observed minimum PBL height was lower than that reported by Haman et al. (2012), likely due to the cloudy conditions prevailing in September 2013. There was no apparent explanation on the reduced daytime PBL biases in the OA case than the base case, but it is likely the results of improved winds and temperatures in PBL.

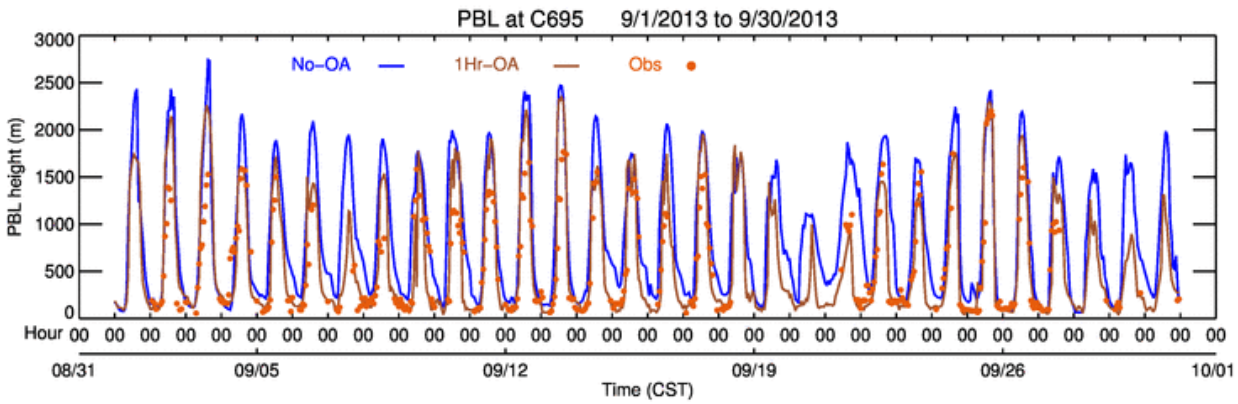

393

394 **Figure 6**. Planetary Boundary Layer (PBL) height time series at CAMS C695 for September
395 2013.

396 **5.1.4. Cold Front Passage**

397 The surface winds on 09/20 were overwhelmingly southerly in the region and reversed on 21
398 September due to the arrival of a cold front. The hour-by-hour wind shifts for 11 sites in HGB on
399 21 September are plotted in Figure 7. The sites are sorted by latitude with the southernmost site,
400 Galveston C1034, located at the bottom row. There was only one site, Deer Park C35, showing
401 weak southerly at 00 CST while all the others had mostly weak northerly. Starting from 01 CST,
402 winds in the entire HGB area turned northerly to northeasterly and continued gaining strength in
403 the next few hours, indicating cold air had taken over the region.

404 Both cases performed reasonably well on 09/21 and the timing of wind shift was captured quite
405 accurately; although "No-OA" lagged behind by ~ 1 hr. The winds turned weak northerly at 00
406 CST for most sites but the "No-OA" case still showed the wind direction to be all southerly.
407 Besides the timing, the northeasterly winds in "No-OA" case sometimes were too strong; obs-
408 nudging helped moderate the winds. The reduced V-wind bias in "1Hr-OA" was also evident in
409 the wind model-measurement statistics on 21 September.

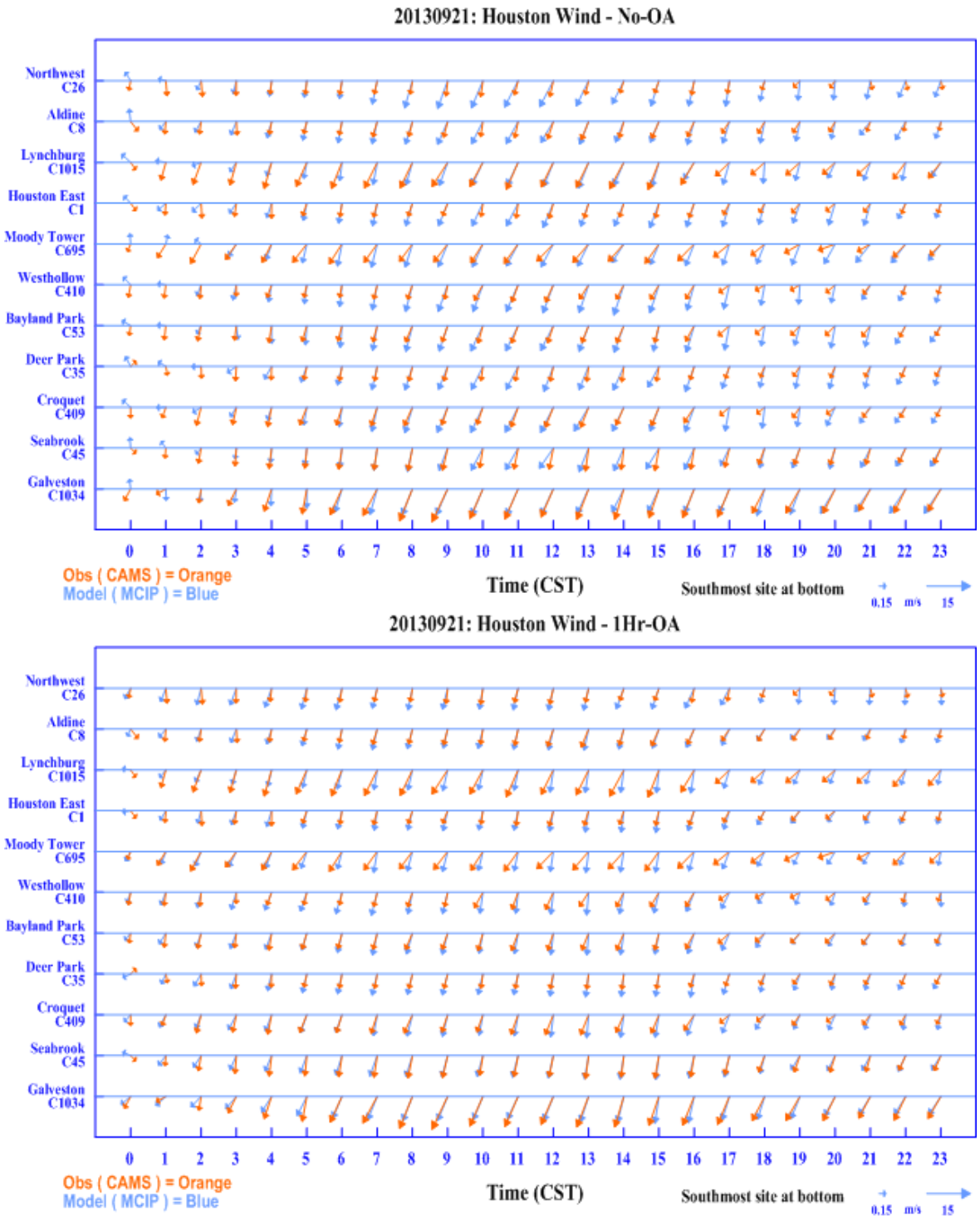

410

411 **Figure 7**. Hourly model (blue) and CAMS (orange) winds at 11 sites on 21 September: No-OA
412 (top) and 1hr-OA (bottom). The 1hr-OA case is better in 00 CST to 02 CST and 17 CST to 20
413 CST.

5.2. Ozone

5.2.1. Regional Average Hourly Ozone

Figure 4 plots the regional average hourly ozone, which was defined similarly to the average temperature. Overall, observed ozone concentrations were low and the model did a reasonably good job on capturing the timing of intra-day variations. However, both cases tended to overpredict the daily highs and daily lows, especially in the first 8 days and between 15 and 21 September. An obvious departure is the 25th – both cases missed the daily high. During the model high bias period, the OA case usually did better in reaching the daily low although it overpredicted the high a bit more than the base case. The night time biases were reduced likely because the lower southerly winds in the OA case transported less ozone from the Gulf to the land.

Our results suggested that the modeled ozone concentrations were likely higher in the Gulf than actual. However during the 2nd – 4th and 7th-8th of September, the incoming ozone from the Gulf was markedly lower. Since the model ozone had fixed boundary values, the model was unable to capture the daily ozone variation at the boundary. The model showed the highest biases during period of the 19th -20th likely due to overcast skies and uncertainties in model's cloud fields and high background ozone values. Despite the overprediction, the biases in OA case are notably lower during the nights of 19th and 20th. A future study to upgrade the accuracy of cloud fraction using remote sensing data (e.g., MODIS) should be helpful in explaining the biases.

There were a few days with elevated ozone due to post-front meteorology conditions. The only exceedance happened on 09/25, which was likely caused by meteorological events in Houston and the Galveston Bay. The overall ozone on 26 September was higher after southerly winds transported back the ozone from the Gulf, raising the ozone level in the entire region. A more detailed analysis of model predictions on 09/25 and 09/26 will be presented in following subsection of 5.2.3.

5.2.2. Performance Statistics

The ozone statistics are listed in Table 4. Both cases had very close correlation of 0.72 and 0.73. However, the mean biases in the OA case were lower by 3.2 ppb, which helped raise the IOA

from 0.78 to 0.83. The model standard deviation increased in the OA case and matched better with that of the in-situ data. The improvement in IOA was slightly less as compared to that for temperature and winds.

5.2.3. High ozone episode after the passage of a front

In SETX, high ozone events during the fall season usually occurred after the passage of a cold front (e.g., Rappenglück et al. 2008; Ngan and Byun 2011; Ngan et al. 2012; Haman et al. 2014). Two factors may have contributed to the post-front ozone events: 1) Following a cold spell, light winds and sunny skies create an ideal condition for ozone production and accumulation. 2) Wind reversal may transport back the pollutants that were previously blown into the Gulf.

During the DISCOVER-AQ period, the two days with highest ozone concentrations were the 25th and 26th of September as indicated in Figure 4. The 1-hour maximum ozone on the 25th was localized and higher by about 40 ppb than the 26th. In addition to heightened background ozone on the 25th, the major contributor was the production resulting from favorable weather conditions: sunny, overall light winds and shifting winds over the industrial area. The light morning land breeze carried pollutants from ship channel area to the Galveston Bay. As the day warmed up, the bay breeze started to develop and carry pollutants back to the land. This localized circulation was described by Banta et al. (2005). Ngan et al. (2012) reported the same phenomenon in their Texas Air Quality Study-II 2006 study.

Figure 8 shows the ozone time series for the La Porte (C556 in Figure 1) site located in the HSC area. The highest hourly ozone for September, 151 ppb occurred here at 13 CST on the 25th. Ozone rose from 10 ppb to 150 ppb between 09-12 CST. Such a dramatic increase in ozone was likely the result of increased photochemical activity under favorable meteorological conditions in an area with accumulated precursors. Figures 9 and 10 depict the wind and ozone concentrations at 08 CST and 13 CST.

The wind plots of Figure 9 indicate that the winds in the HGB region at 8 CST were light northerly for sites located on the north side while they were westerly for the sites in the middle and south. The base case winds were all northerly while the OA case had northwest winds for north side and west winds for the middle and south. Hence, the model winds in OA case are more realistic than the winds in base case. The 09 CST winds were similar to those of 08 CST.

As a result, the ozone statistics in Table 5 showed that the OA case had much better correlation and IOA than the base case during 08-09 CST. This example demonstrated the ability of obs-nudging to correct erroneous winds. However, later events showed it may not always be able to perform consistently.

The bay breeze started to develop at 10 CST near the C556 site. The early onset was likely to be related to warming up on the previous afternoon on 09/24 as indicated in Figure 3. At 10 CST most other sites to the west of HSC experienced light northwest winds while those at HSC originated from the northeast. Combined with the easterly bay breeze, a convergence zone was formed just below C556, where emissions from the HSC area stalled and accumulated. At 13 CST, the whole region had light winds and the bay breeze was well developed. The highest ozone indeed appeared in C556 and its vicinity. The rapid increase of ozone concentration for C556 between 09-13 CST is shown in Figure 8.

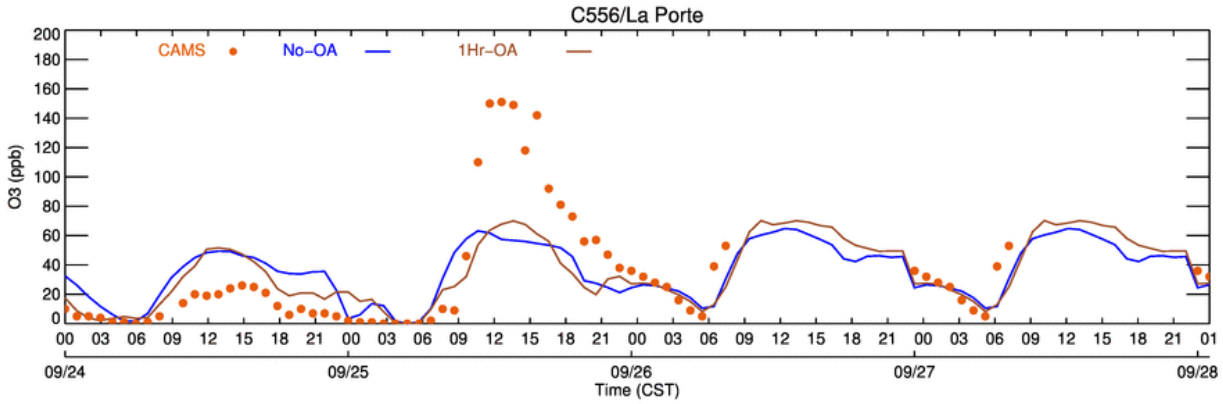

Figure 8. Ozone time series of La Porte (C556) between 09/24_00 to 09/28_00 CST of 2013.

It is important to note that both modeled cases missed the wind shifts in the HSC area, and the resulting convergence zone near C556. This could explain the model's inability to recreate the sharp ozone increase at C556. Figure 9 shows that the ozone concentrations around HSC area are quite low (~10 ppb) at 08 CST. A further examination showed that while both model cases missed the wind shift and convergence, the patterns were different. The base case had flawed winds for most of the morning: instead of a weak westerly, it had stronger northwesterly to northerly. By 08 CST, winds were almost uniformly northerly in the base case while they were weak west-northwesterly in the OA case (Figure 9). The oval in Figure 9's top-left panel shows

493 the mismatch of winds around C556 in the base case. As a result, the NO_x produced in the city
494 was carried further to the southeast in the model in the base case. Until 13 CST, base case winds
495 did not shift directions by much. The OA case got the early hour weak northwesterly right, but
496 missed the bay breeze onset between 10 and 13 CST (oval in Figure 10). The OA case could not
497 reproduce the small-scale wind reversal near C556, suggesting there is a limitation in the current
498 WRF OA's capability. On the other hand, the OA case did improve the spatial ozone pattern, as
499 the high ozone area was closer to HSC after OA (Figure 10).

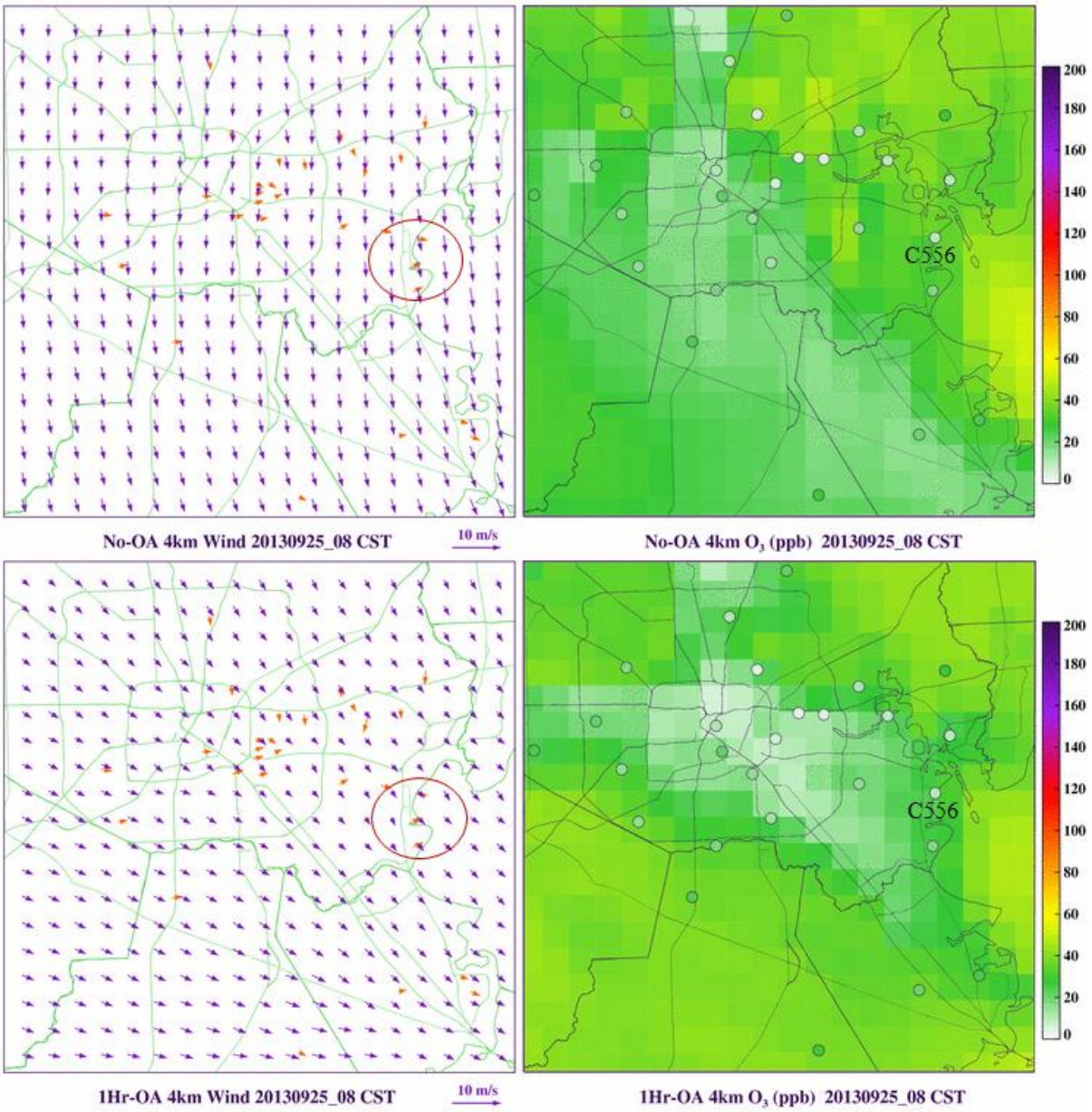

500

Figure 9. Zoom-in ozone concentrations (right) and wind plots (left) at 13 CST 25 September for "No-OA" (top) and "1Hr-OA" (bottom). Ozone observation is in small circle; wind observation is indicated by an orange arrow. La Porte site C556 is labeled. The numerical range of right-side colour scale is 0 to 200 ppb. Higher value than 200 ppb has the same colour as 200 ppb.

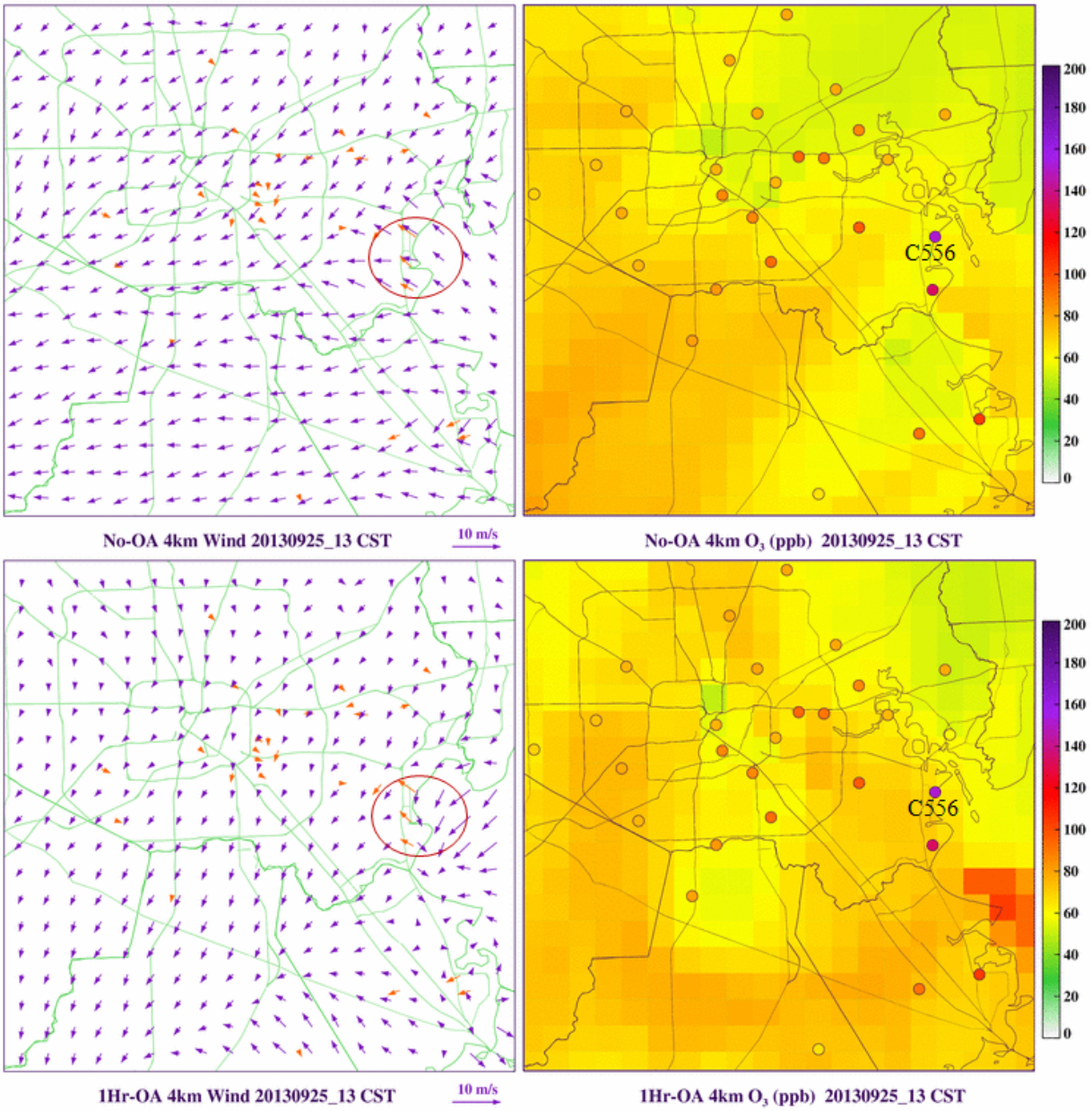

Figure 10. Zoom-in ozone concentrations (right) and wind plots (left) at 13 CST 25 September for "No-OA" (top) and "1Hr-OA" (bottom). Ozone observation is in small circle; wind observation is indicated by an orange arrow. Bay breeze is shown in the orange oval.

The ozone measurements from aircraft P3-B provided a more complete picture for the ozone evolution on 09/25. During the day, the aircraft flew around the industrial area, Galveston Bay and Galveston Island for about 9 hours. Figures 11 and 12 plot the ozone concentrations along aircraft tracks at 08 and 13 CST. Surface layer ozone from the "No-OA" case is provided as background for reference. At 08 CST, ozone level of 60-80 ppb aloft was already observed at three locations (three loops in Fig.11): Galveston Island, Smith Point and inner city. Another high of ~90 ppb could be seen above the HSC area. Ozonesonde observations over HGB showed the aloft ozone concentrations were typically ~40-50 ppb (e. g., Li and Rappengluck 2014) at the height level. The higher-than normal ozone aloft suggested a post-front ozone recirculation condition. Such high ozone aloft might raise surface ozone as a growing PBL downwardly mixed the air aloft with near surface air. At 13 CST, high ozone over 100 ppb was observed at multiple locations. The highest aloft ozone of ~ 160 ppb occurred southwest of Smith Point in the Galveston Bay. Such high increase in ozone concentrations was likely the result of active photochemistry in the industrial zone and around Galveston Bay; indicating a high level of precursor accumulation in the area.

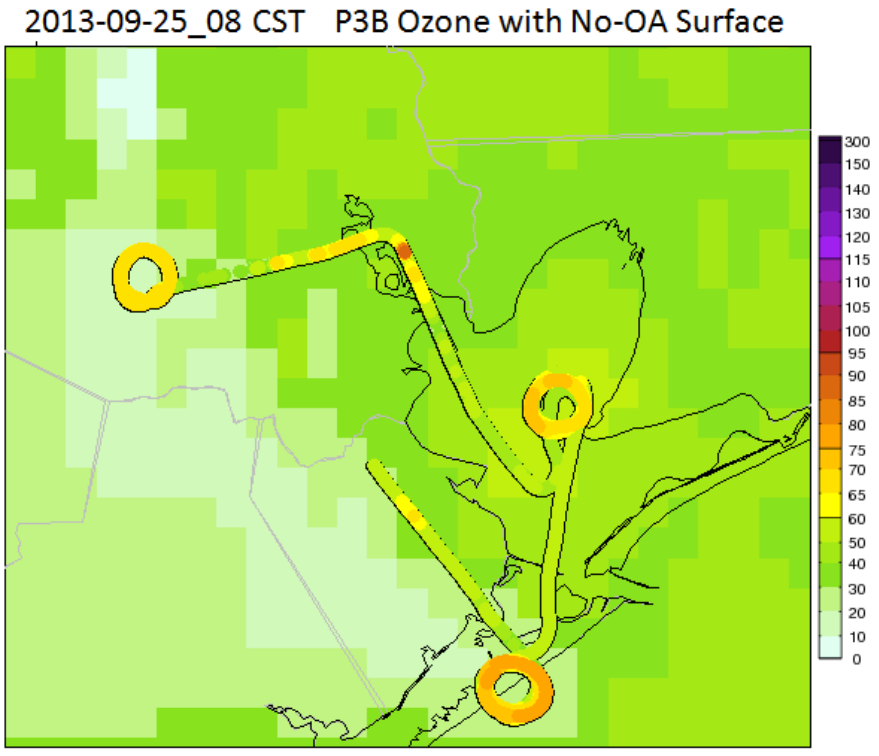

Figure 11. Ozone along aircraft tracks at 08 CST of September 25th, overlaid upon model No-OA surface ozone.

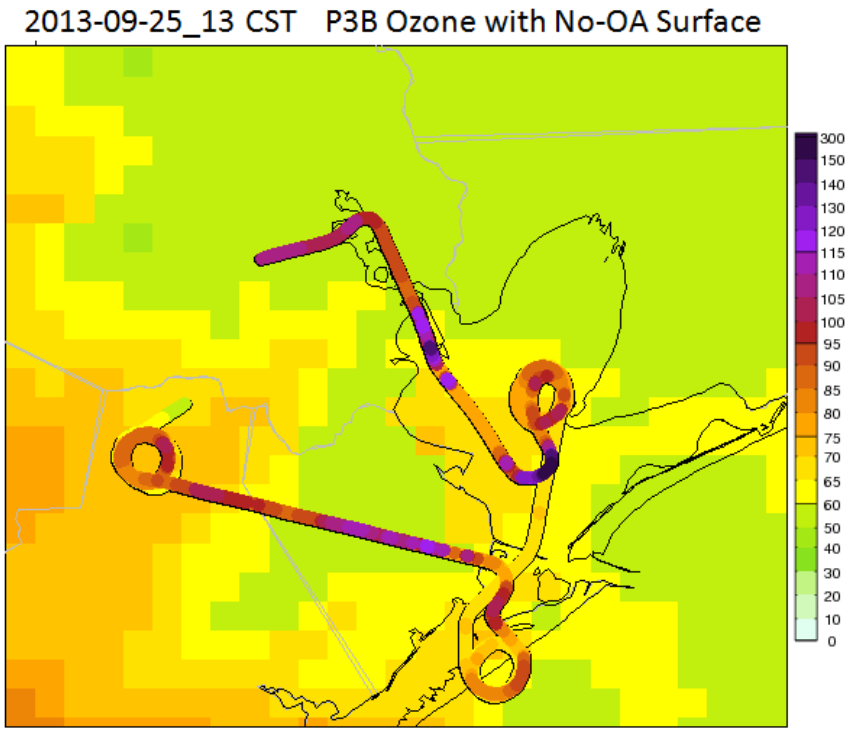

Figure 12. Ozone along aircraft tracks at 09/25_13 CST of September 25th, overlaid upon model "No-OA" surface ozone. Plumes can be seen as dark purple circles in Galveston Bay.

Figure 13 shows hourly ozone vertical profiles from 08 CST to 16 CST on September 25th, with ozone being displayed on the x-axis and height on the y-axis. The observed ozone was averaged over multiple measurements in the same model cell, so that they could be compared to model output. Next, both model and observed ozone values were averaged over all the grid cells in the same model layer, such that one dot represents the average ozone of all the cells in the same layer. The 08 and 09 CST profiles showed there was a high ozone layer with average ozone of ~65 ppb stretching from 450 m to 1200 m height. In comparison, all model runs had lower ozone in this layer. The model biases as shown in Figure 14 were about -10 ppb at 08 CST and grew to -20 ppb at 09 CST. The large discrepancy between low surface ozone and ozone aloft was unusual and may be explained by the arrival of high ozone air mass aloft. The observed ozone rose continuously in following hours yet model simulated ozone stagnated around 60 ppb from surface up to 2000 m until 15 CST. At 16 CST, the ozone of OA case in the lowermost (0-1 km)

layer rose 20 ppb over the previous hours yet the base case ozone increased only a few ppb. Although different in magnitude, the aloft ozone had a few similar features to the surface ozone. Firstly, the model missed the observed high ozone in the afternoon by a large margin. For example, the base case underpredicted the 0-1 km level ozone by up to 50 ppb. The primary cause for the lower ozone production was likely model's wind fields as both model and observations had a clear sky in industrial area and Galveston Bay. Secondly, nudging clearly helped reducing the ozone biases aloft. In most plots of Figure 14, the OA case had lower biases than the base case. The largest difference was at 16 CST when nudging reduced biases from ~45 ppb to ~30 ppb in the 300 – 1000 m layer.

While it is easy to understand the improvements in temperature and winds after obs-nudging was applied, it is more difficult to explain how other variables such as precipitation and clouds reacted to obs-nudging. The indirect impact of these meteorological variables on ozone was harder to assess. In our study, we did not evaluate clouds quantitatively as there were no digitized cloud fraction data available for our modeling domains. A preliminary analysis on convection showed that there were occasions in which model missed the convection or precipitation and there were other occasions in which model created artificial convection. The convection cells were usually visible as "star-burst" from surface wind vector plots – arrows going out to different directions from a center. However, the mismatch in convection appeared to be not a serious issue since only a few occurrences were observed in the month of September.

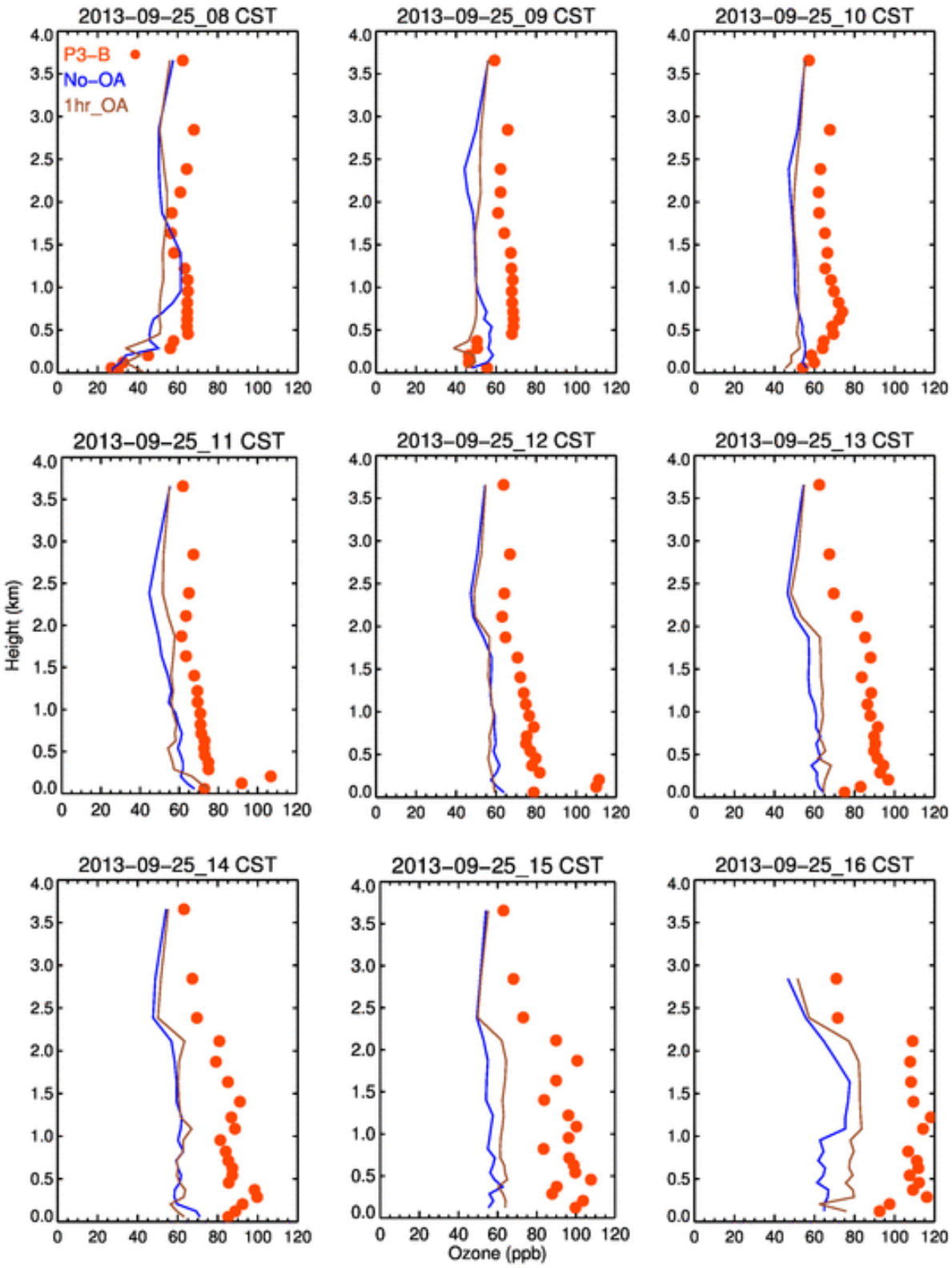

563

564 **Figure 13**. Vertical ozone profiles from 09/25_08 CST to 09/25_16 CST of 2013 for two cases
565 of No-OA and 1Hr-OA compared with corresponding observations.

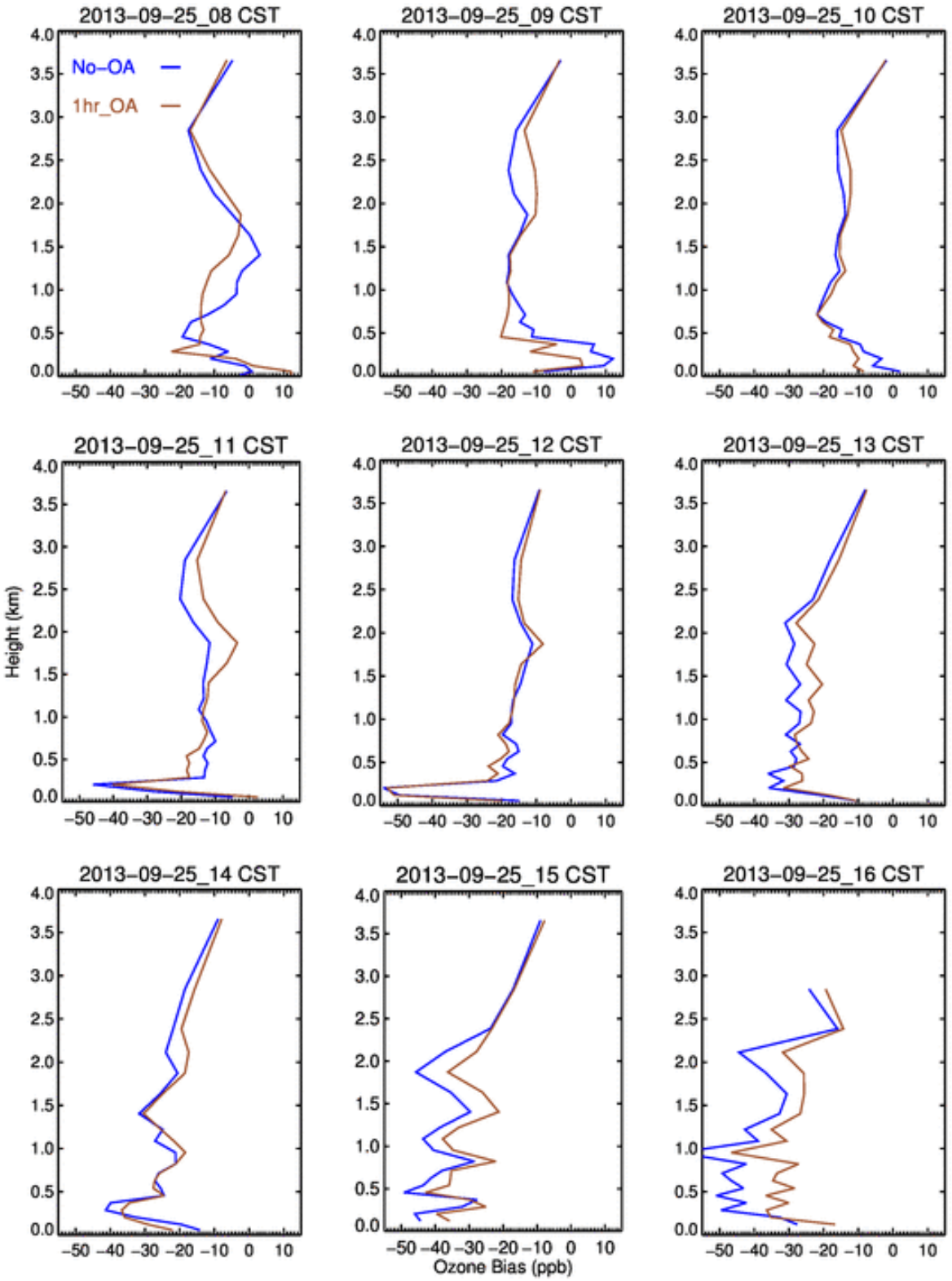

566

567 **Figure 14**. Model vertical ozone biases from 09/25_08 CST to 09/25_16 CST of 2013 for two
568 cases of No-OA and 1Hr-OA.

6. Conclusions and Discussions

In this study, we performed two Weather Research and Forecasting (WRF) and Community Multiscale Air Quality (CMAQ) model simulations to explore model sensitivity to observation nudging. In evaluating meteorological and ozone conditions, we found that obs-nudging improved the meteorology and ozone performance as shown in the index of agreement (IOA) of temperature, winds, and ozone. While the base case winds were overall well simulated, obs-nudging significantly reduced the high wind biases (especially the meridional wind) shown in the base case. For planetary boundary layer height, obs-nudging reduced high biases in both daily maximum and daily minimum values. In the end, the combined changes in meteorology lowered the ozone biases by about 3 ppb, a 35% reduction. There were short time periods (such as between 07 and 09 CST on 09/25) when the simulated base case model winds differed significantly from observational data and obs-nudging significantly corrected the meteorological simulation problems, leading to much better ozone simulation. However, model ozone biases are also impacted by emissions and lateral boundary conditions.

The only high ozone episode in the simulation period was related to the cold front passage. The small-scale winds and high aloft ozone concentrations on 09/25 likely contributed to the ozone exceedance in the area. It is also possible that an unreported emission event played a role. Since the maximum surface ozone at La Porte was much higher than the morning-time aloft ozone, the active local ozone production was likely the dominant factor. Analyses of aloft ozone on 09/25 showed while there was high aloft ozone and large negative model biases, the OA case tended to have smaller biases, especially in late hours.

Small-scale meteorological events are frequently cited for their contributions to high ozone events. Model's capability in reproducing these events is critical in simulating such high ozone episodes. The base case did not recreate the 25 September small-scale events likely due to the complex winds and a lack of local information which can be used to steer model state closer to reality. On the other hand, the inability of the sensitivity case to replicate the local winds is likely a result of the imperfection of the nudging process pending further investigation. An ongoing study by the current authors suggests that errors in the metrological fields from the default grid nudging files are important sources. Methods are being tested to improve the quality of grid nudging files. Early results showed that the bay breeze which caused the wind reversal around La

Porte was well captured through improved grid nudging files. In addition, more observational data (e.g., more sites and higher data frequency) and more testing on the combination of nudging setting should help improve the obs-nudging performance. Also, the impact of obs-nudging on precipitation and clouds should be further investigated to understand their chain effect on chemistry.

Acknowledgements

The authors thank Texas Air Research Center (TARC) for its support through grant number 413UHH0144A and Air Quality Research Program (AQRP) through 14-014, the DISCOVER-AQ team for the aircraft data, Vanessa Caicedo for LIDAR data, and the TCEQ CAMS site team for the in-situ ozone and meteorological data.

References

Banta, R. M., Senff, C. J., White, A. B., Trainer, M., McNider, R. T., Valente, R. J., Mayor, S. D., Alvarez, R. J., Hardesty, R. M., and Parrish, D.: Daytime buildup and nighttime transport of urban ozone in the boundary layer during a stagnation episode, J. Geophys. Res.-Atmos., 103, 22519-22544, 1998.

Banta, R. M., Senff, C. J., Nielsen-Gammon, J., Darby, L. S., Ryerson, T. B., Alvarez, R. J., Sandberg, S. R., Williams, E. J., and Trainer, M.: A bad air day in Houston, B. Am. Meteorol. Soc., 86, 657-669, doi:10.1175/bams-86-5-657, 2005.

Banta, R. M., Senff, C. J., Alvarez, R. J., Langford, A. O., Parrish, D. D., Trainer, M. K., Darby, L. S., Hardesty, R. M., Lambeth, B., Neuman, J. A., Angevine, W. M., Nielsen-Gammon, J., Sandberg, S. P., and White, A. B.: Dependence of daily peak O_3 concentrations near Houston, Texas on environmental factors: Wind speed, temperature, and boundary-layer depth, Atmos. Environ., 45, 162-173, doi:10.1016/j.atmosenv.2010.09.030, 2011.

Byun, D., and Schere, K. L.: Review of the governing equations, computational algorithms, and other components of the models-3 Community Multiscale Air Quality (CMAQ) modeling system, Appl. Mech. Rev., 59, 51-77, doi:10.1115/1.2128636, 2006.

Byun, D., Ngan, F., Li, X., Lee, D., Kim, S..: "Analysis of Air Pollution Events in Summer 2006 and Preparation of Model Input Data for the Assessment Study", Grant No. 582-5-64594- FY07-02, Final Report: Evaluation of Retrospective MM5 and CMAQ Simulations of TexAQS-II Period with CAMS Measurements, Texas Commission on Environmental Quality, February 2008, 25 pp

Cheng, F.Y., and Byun, D. : Application of high resolution land use and land cover data for atmospheric modeling in the Houston-Galveston metropolitan area, Part I: Meteorological simulation results, Atmos. Env., 42, 7795-7811, doi:10.1016/j.atmosenv.2008.04.055, 2008.

Cheung, V. T., and Wang, T.: Observational study of ozone pollution at a rural site in the Yangtze Delta of China, Atmos. Env., 35, 4947-4958, 2001.

635 Choi, Y.: The impact of satellite-adjusted NO_x emissions on simulated NO_x and O_3 discrepancies
636 in the urban and outflow areas of the Pacific and Lower Middle US, Atmos. Chem. Phys., 14,
637 675-690, doi:10.5194/acp-14-675-2014, 2014.

638 Choi, Y. and Souri, A.: Chemical condition and surface ozone in large cities of Texas during the
639 last decade: observational evidence from OMI, CAMS, and Model Analysis, Remote Sensing of
640 Environ., 168:90-101, doi:10.1016/j.rse.2015.06.026, 2015

641 Choi, Y., Kim, H., Tong, D., and Lee, P.: Summertime weekly cycles of observed and modeled
642 NO_x and O_3 concentrations as a function of satellite-derived ozone production sensitivity and
643 land use types over the Continental United States, Atmos. Chem. Phys., 12, 6291-6307,
644 doi:10.5194/acp-12-6291-2012, 2012

645 Cuchiara, G. C., Li, X., Carvalho, J., and Rappengl ̈uck, B.: Intercomparison of planetary
646 boundary layer parameterization and its impacts on surface ozone concentration in the
647 WRF/chem model for a case study in Houston, Texas, Atmos. Environ., 175-185,
648 doi:10.1016/j.atmosenv.2014.07.013, 2014.

649 Czader, B. H., Li, X. S., and Rappenglueck, B.: CMAQ modeling and analysis of radicals,
650 radical precursors, and chemical transformations, J. Geophys. Res.-Atmos., 118, 11376-11387,
651 doi:10.1002/Jgrd.50807, 2013.

652 Czader, B.H., Choi, Y., Li, X., Alvarez, S., Lefer, B.: Impact of updated traffic emissions on
653 HONO mixing ratios simulated for urban site in Houston, Texas. Atmos. Chem. Phys., 15(3),
654 1253-1263, doi:10.5194/acp-15-1253-2015, 2015.

655 Darby, L. S.: Cluster analysis of surface winds in Houston, Texas, and the impact of wind
656 patterns on ozone, J. Appl. Meteorol., 44, 1788-1806, doi:10.1175/jam2320.1, 2005.

657 Daum, P. H., Kleinman, L. I., Springston, S. R., Nunnermacker, L. J., Lee, Y. N., Weinstein-
658 Lloyd, J., Zheng, J., and Berkowitz, C. M.: Origin and properties of plumes of high ozone
659 observed during the Texas 2000 Air Quality Study (TexAQS 2000), J. Geophys. Res.-Atmos.,
660 109, D17306, doi:10.1029/2003jd004311, 2004.

Deng, A., Stauffer, D., Gaudet, B., Dudhia, J., Hacker, J., Bruyere, C., Wu, W., Vandenberghe, F., Liu, Y., Bourgeois, A.: Update on WRF-ARW End-to-end Multi-scale FDDA System. 10th WRF Users' Workshop, Boulder, CO, NCAR, 2009

Foley, K. M., Roselle, S. J., Appel, K. W., Bhave, P. V., Pleim, J. E., Otte, T. L., Mathur, R., Sarwar, G., Young, J. O., Gilliam, R. C., Nolte, C. G., Kelly, J. T., Gilliland, A. B., and Bash, J. O.: Incremental testing of the Community Multiscale Air Quality (CMAQ) modeling system version 4.7, Geosc. Model Development, 3, 205-226, doi:10.5194/gmd-3-205-2010, 2010.

Gilliam, R. C., and Pleim, J. E.: Performance Assessment of New Land Surface and Planetary Boundary Layer Physics in the WRF-ARW, J. Appl. Meteorol. Climatol., 49, 760-774, doi:10.1175/2009jamc2126.1, 2010.

Haman, C.L., Lefer, B., Morris, G.A.: Seasonal Variability in the Diurnal Evolution of the Boundary Layer in a Near-Coastal Urban Environment. J. Atmos. Ocean Tech., 29, 697-710, 2012.

Haman, C.L., Couzo, E., Flynn, J.H., Vizuete, W., Heffron, B., Lefer, B.L.: Relationship between boundary layer heights and growth rates with ground-level ozone in Houston, Texas. J Geophys Res-Atmos., 119, 6230-6245, 2014.

Houyoux, M., Vukovich, J., Brandmeyer, J., 2000. Sparse Matrix Kernel Emissions Modeling System: SMOKE User Manual. MCNC-North Carolina Supercomputing Center. Available at: https://cmascenter.org/smoke/.

Huang, X.-Y., Xiao, Q., Barker, D. M., Zhang, X., Michalakes, J., Huang, W., Henderson, T., Bray, J., Chen, Y., and Ma, Z.: Four-dimensional variational data assimilation for WRF: Formulation and preliminary results, Mon. Weather Rev., 137, 299-314, 2009.

Kleinman, L. I., Daum, P. H., Lee, Y. N., Nunnermacker, L. J., Springston, S. R., Weinstein-Lloyd, J., and Rudolph, J.: Ozone production efficiency in an urban area, J Geophys Res.-Atmos, 107, 4733, doi:10.1029/2002jd002529, 2002.

Le Dimet, F.X. and Talagrand, O.: Variational algorithms for analysis and assimilation of meteorological observations: theoretical aspects, Tellus, 38A, 97–110, 1986.

688 Li, X., and Rappenglück, B.: A WRF–CMAQ study on spring time vertical ozone structure in
689 Southeast Texas, Atmos. Environ., 97, 363-385, doi:10.1016/j.atmosenv.2014.08.036, 2014.

690 Li, X., Lee, D., Kim, S.-T., Kim, H., Ngan, F., Cheng, F., and Byun, D.: Performance
691 Evaluation of a Year-long Run of an Air Quality Forecasting System for Southeast Texas,
692 10th Conference on Atmospheric Chemistry, New Orleans, January 2008, 2008.

693 Liu, Y., Bourgeois, A., Warner, T., Swerdlin, S., and Hacker, J.: An implementation of
694 observation nudging-based FDDA into WRF for supporting ATEC test operations, 2005 WRF
695 user workshop, Boulder, CO, 2005.

696 Liu, Y., Bourgeois, A., Warner, T., Swerdlin, S., and Yu, W.: An update on "observation
697 nudging"-based FDDA for WRF-ARW: Verification using OSSE and performance of real-time
698 forecasts, 2006 WRF user workshop, Boulder, CO, 2006.

699 Ngan, F., Byun, D., Kim, H., Lee, D., Rappengluck, B., and Pour-Biazar, A.: Performance
700 assessment of retrospective meteorological inputs for use in air quality modeling during TexAQS
701 2006, Atmos. Environ., 54, 86-96, doi:10.1016/j.atmosenv.2012.01.035, 2012.

702 Mason, R.; Strum, M.; Houyoux, M. Technical Support Document (TSD) Preparation of
703 Emissions Inventories for the Version 4, 2005-based Platform; U.S. Environmental Protection
704 Agency, Office of Air and Radiation, Office of Air Quality Planning and Standards, Air Quality
705 Assessment Division, 2010

706 Olaguer, E. P., Rappengluck, B., Lefer, B., Stutz, J., Dibb, J., Griffin, R., Brune, W. H., Shauck,
707 M., Buhr, M., Jeffries, H., Vizuete, W., and Pinto, J. P.: Deciphering the Role of Radical
708 Precursors during the Second Texas Air Quality Study, J. Air & Waste Manag. Assoc., 59, 1258-
709 1277, doi:10.3155/1047-3289.59.11.1258, 2009.

710 Otte, T. L.: The impact of nudging in the meteorological model for retrospective air quality
711 simulations. Part I: Evaluation against national observation networks, J. Applied Meteorol.
712 Climatol., 47, 1853-1867, doi:10.1175/2007jamc1790.1, 2008.

713 Pan, S., Choi, Y., Roy, A., Li, X., Jeon, W., and Souri, A.: Modeling the uncertainty of several
714 VOC and ints impact on simulated VOC and ozone in Houston, Texas, Atmos. Environ., 120,
715 404-416, 2015

716 Parrish, D. D., Allen, D. T., Bates, T. S., Estes, M., Fehsenfeld, F. C., Feingold, G., Ferrare, R.,
717 Hardesty, R. M., Meagher, J. F., Nielsen-Gammon, J. W., Pierce, R. B., Ryerson, T. B., Seinfeld,
718 J. H., and Williams, E. J.: Overview of the Second Texas Air Quality Study (TexAQS II) and the
719 Gulf of Mexico Atmospheric Composition and Climate Study (GoMACCS), J. Geophys. Res.-
720 Atmos., 114, doi:10.1029/2009jd011842, 2009.

721 Pour-Biazar, A., McNider, R. T., Roselle, S. J., Suggs, R., Jedlovec, G., Byun, D. W., Kim, S.,
722 Lin, C. J., Ho, T. C., Haines, S., Dornblaser, B., and Cameron, R.: Correcting photolysis rates on
723 the basis of satellite observed clouds, J. Geophys. Res.-Atmos., 112, D10302,
724 doi:10.1029/2006jd007422, 2007.

725 Rappengluck, B., Perna, R., Zhong, S. Y., and Morris, G. A.: An analysis of the vertical structure
726 of the atmosphere and the upper-level meteorology and their impact on surface ozone levels in
727 Houston, Texas, J. Geophys. Res.-Atmos., 113, doi:10.1029/2007jd009745, 2008.

728 Rappenglück, B., Lefer, B., Mellqvist, J., Czader, B., Golovko, J., Li, X., Alvarez, S., Haman,
729 C., and Johansson, J., 2011: University of Houston Study of Houston Atmospheric Radical
730 Precursors (SHARP), Report to the Texas Commission on Environmental Quality, August 2011,
731 145 pp

732 Skamarock, W. C., Klemp, J. B., Dudhia, J., Gill, D. O., Barker, M., Duda, K. G., Huang, Y.,
733 Wang, W., and Powers, J. G.: A description of the Advanced Research WRF Version 3, 1-113,
734 2008.

735 Stauffer, D. R., and Seaman, N. L.: Use of 4-dimensional data assimilation in a limited-area
736 mesoscale model .1. Experiments with synoptic-scale data, Mon. Weather Rev., 118, 1250-1277,
737 1990.

738 Stauffer, D. R., and Seaman, N. L.: Multiscale 4-dimensional data assimilation, J. Appl.
739 Meteorol., 33, 416-434, 1994.

Tucker, S. C., R. M. Banta, A. O. Langford, C. J. Senff, W. A. Brewer, EJ. Williams, B. M. Lerner, H. D. Osthoff, and R. M. Hardesty. : Relationships of coastal nocturnal boundary layer winds and turbulence to Houston ozone concentrations during TexAQS 2006. Journal of Geophysical Research: Atmospheres, 115, no. D10 (2010).

Willmott, C. J.: On the Validation of Models, Physical Geography, 2, 184-194, doi:10.1080/02723646.1981.10642213, 1981.

Zhong, S. Y., In, H. J., and Clements, C.: Impact of turbulence, land surface, and radiation parameterizations on simulated boundary layer properties in a coastal environment, J. Geophys. Res.-Atmos., 112, doi:10.1029/2006jd008274, 2007.

Table 1. Major WRF physics and FDDA Options, the numbers in the parentheses are the related settings in WRF namelist file.

WRF Version	V3.5.1
Microphysics	Lin et al Scheme
Long-wave Radiation	RRTMG
Short-wave Radiation	New Goddard scheme
Surface Layer Option	Monin-Obukhov with CB viscous sublayer scheme
Land-Surface Option	Unified Noah LSM
Urban Physics	None
Boundary Layer Scheme	YSU
Cumulus Cloud Option	Kain-Fritsch
FDDA	Grid nudging on for all; Observation-nudging on for the OA case

Table 2. Major CMAQ Options, the text in the parentheses are the related settings in CMAQ build script.

CMAQ version	V5.0.1
Chemical Mechanism	CB05 gas-phase mechanism with active chlorine chemistry, updated toluene mechanism, fifth-generation CMAQ aerosol mechanism with sea salt, aqueous/cloud chemistry
Lightning NOx emission	Included inline
Horizontal advection	YAMO (Yamartino)
Vertical advection	WRF omega formula
Horizontal mixing/diffusion	Multiscale
Vertical mixing/diffusion	Asymmetric Convective Model (ACM) version 2
Chemistry solver	EBI (Euler Backward Iterative)
Aerosol	AERO5 for sea salt and thermodynamics
Cloud Option	ACM cloud processor for AERO5
Boundary conditions	Default static profiles

Table 3 Statistics of surface T, U-wind and V-wind for three WRF simulations: N – data points; Corr – Correlation; IOA – Index of Agreement; RMSE – Root Mean Square Error; MAE – Mean Absolute Error; MB – Mean Bias; O – Observation; M - Model; O_M – Observed Mean; M_M – Model Mean; SD – Standard Deviation; Units for RMSE/MAE/MB/O_M/M_M/O_SD/M_SD: degree C

Surface temperature T										
Case	N	Corr	IOA	RMSE	MAE	MB	O_M	M_M	O_SD	M_SD

No-OA	41058	0.83	0.89	2.0	1.5	0.9	27.4	28.3	3.1	2.8
1Hr-OA	41058	0.94	0.97	1.0	0.8	0.0	27.4	27.4	3.1	3.1
Surface U wind										
Case	N	Corr	IOA	RMSE	MAE	MB	O_M	M_M	O_SD	M_SD
No-OA	43246	0.76	0.84	1.4	1.1	-0.6	-1.3	-1.9	1.6	1.9
1Hr-OA	43246	0.81	0.89	1.0	0.8	-0.3	-1.3	-1.6	1.6	1.6
Surface V wind										
Case	N	Corr	IOA	RMSE	MAE	MB	O_M	M_M	O_SD	M_SD
No-OA	43246	0.76	0.8	2.1	1.7	1.2	0.4	1.7	2.0	2.6
1Hr-OA	43246	0.80	0.89	1.2	0.9	-0.1	0.4	0.4	2.0	2.0

764

765 Table 4 Statistics of ozone for CMAQ simulations, see table 3 for column header information

Case	N	Corr	IOA	RMSE	MAE	MB	O_M	M_M	O_SD	M_SD
No-OA	33308	0.72	0.78	14.9	12.3	9.3	24.4	33.7	16.5	14.1
1Hr-OA	33308	0.73	0.83	13.8	11.0	6.1	24.4	30.6	16.5	17.4

766

Table 5 Statistics of ozone on 09/25/2013, all day and hour 0 to 13. Both correlation and index of agreement are unitless. The red numbers indicate the three hours (07 CST to 09 CST) when the ozone in 1Hr-OA case is significantly better than the No-OA case due to much improved winds.

		No-OA		1Hr-OA	
	N	Corr	IOA	Corr	IOA
Hr|All	1150	0.79	0.86	0.81	0.88
0	48	0.04	0.30	0.40	0.46
1	43	0.20	0.24	0.36	0.30
2	48	0.14	0.25	0.35	0.35
3	48	0.19	0.30	0.32	0.35
4	48	0.27	0.36	0.31	0.35
5	47	0.24	0.36	0.28	0.37
6	47	0.33	0.38	0.35	0.37
7	48	0.06	0.39	0.29	0.47
8	48	0.09	0.43	0.53	0.63
9	47	0.05	0.41	0.55	0.74
10	47	-0.10	0.29	0.30	0.51
11	47	0.13	0.39	-0.07	0.36
12	49	0.09	0.38	0.25	0.40
13	49	-0.09	0.37	0.36	0.46